Available online at www.sciencedirect.com

ScienceDirect

Geochimica et Cosmochimica Acta 250 (2019) 1–17

Geochimica et Cosmochimica Acta

www.elsevier.com/locate/gca

Effects of early diagenesis on Mg isotopes in dolomite: The roles of Mn(IV)-reduction and recrystallization

Weiqiang Li [a,*], Or M. Bialik [b,*], Xiaomin Wang [a], Tao Yang [a], Zhongya Hu [a], Qingyu Huang [a], Shugao Zhao [a], Nicolas D. Waldmann [b]

[a] *State Key Laboratory for Mineral Deposits Research, School of Earth Sciences and Engineering, Nanjing University, Nanjing, Jiangsu 210093, PR China*

[b] *The Dr. Moses Strauss Department of Marine Geosciences, Charney School of Marine Sciences, University of Haifa, Mount Carmel, 31905 Haifa, Israel*

Received 10 May 2018; accepted in revised form 14 January 2019; available online 29 January 2019

Abstract

Sedimentary dolomite plays an important role in global Mg cycling, and Mg isotopes in massive dolostones may be used to infer secular changes in seawater chemistry through geological history. However, sedimentary dolomite is generally regarded as a diagenetic product, and many details about the effects of early diagenesis on the Mg isotope composition of dolomite remain unclear. The mid-Cretaceous (Albian) Soreq and Givat Ye'arim formations near Jerusalem, Israel, contain exceptionally well-preserved massive dolostones, which provide an ideal opportunity to investigate the Mg isotope responses to early diagenesis. Dolomite samples from this section show large variations in $\delta^{13}C$ values and Mn contents that are negatively correlated, reflecting degradation of organic matter and mineralization of organic carbon in the Mn(IV) reduction zone within soft sediment during dolomite formation. This is a rare example of a clear link between Mn(IV) reduction and dolomite precipitation based on geochemical evidence in the rock record. The dolomite samples also exhibit large variations in *d*(104) values and the degree of cation ordering. The latter is negatively correlated with Sr contents, implying that variable degrees of dolomite recrystallization occurred during diagenesis. $\delta^{26}Mg$ values of >50 dolomite samples from this section vary from −2.28‰ to −1.78‰, but do not correlate with indicators of organic matter degradation ($\delta^{13}C$ values and Mn contents) or dolomite recrystallization (e.g., Sr contents), suggesting that Mg isotopes behave conservatively after initial dolomite (or proto-dolomite) precipitation during the very early stages of diagenesis. We propose that the Mg isotope composition of dolomite formed due to Mn(IV) reduction is buffered by seawater due to the shallowness of the Mn(IV) reduction zone in platform sediments, which is different from the dolomitization associated with bacterial sulfate reduction or methanogenesis, where Mg supply can be diffusion-limited. Furthermore, Mg isotopes in dolomite are robust to resetting by recrystallization during burial. Magnesium isotope compositions of platform dolomite that show variable and negatively correlated $\delta^{13}C$ values and Mn contents can, therefore, be considered robust archives for reconstructing paleo-seawater Mg isotope compositions. The variation in $\delta^{26}Mg$ values of the dolostones in the Soreq and Givat Ye'arim formations is interpreted to reflect Rayleigh fractionation in response to dolomitization in a restricted water body. Therefore, the lowest $\delta^{26}Mg$ value is considered to be the Mg isotope composition of dolomite that was in equilibrium with coeval seawater in the open ocean, and thus the $\delta^{26}Mg$ value of Albian seawater was around −0.4‰.

Keywords: Mg isotope; dolomite; early diagenesis; Mn(IV) reduction; recrystallization

* Corresponding authors.
E-mail addresses: liweiqiang@nju.edu.cn (W. Li), obialik@campus.haifa.ac.il (O.M. Bialik).

https://doi.org/10.1016/j.gca.2019.01.029
0016-7037/

1. INTRODUCTION

Dolomite is a major sedimentary reservoir of Mg and dolomitization has an important role in global cycling of Mg (Wilkinson and Algeo, 1989; Arvidson et al., 2011). The chemical composition of seawater, particularly Mg/Ca ratios, is controlled mainly by the balance between riverine input, hydrothermal circulation at mid-ocean ridges, and dolomite precipitation (Hardie, 1996; Tipper et al., 2006). The secular variation of seawater Mg/Ca ratios throughout the Phanerozoic (Broecker, 1971; Hardie, 1996; Holland, 2005; Ries, 2006; Coggon et al., 2010; Gothmann et al., 2015) has been attributed to either changes in intensity of dolomitization over geological time (Wilkinson and Algeo, 1989; Holland, 2005) or variations in the intensity of mid-ocean ridge hydrothermal activity (Elderfield and Schultz, 1996; Hardie, 1996).

The cycling of Mg between seawater, igneous rocks, and marine sediments is accompanied by fractionation of Mg isotopes (Teng, 2017 and references therein), and among all the processes in which Mg cycling is involved, the most significant Mg isotope fractionation is associated with precipitation of carbonate minerals, including calcite (Li et al., 2012; Saulnier et al., 2012; Mavromatis et al., 2013) and dolomite (Higgins and Schrag, 2010; Fantle and Higgins, 2014; Li et al., 2015). Magnesium isotope fractionations between carbonate minerals and aqueous solutions have been progressively better understood through experiments (Li et al., 2012; 2015; Mavromatis et al., 2013; 2017b; Saulnier et al., 2012; Wang et al., 2013), theoretical calculations (Rustad et al., 2010; Schauble, 2011; Pinilla et al., 2015; Wang et al., 2017), and observations of natural samples (e.g., Higgins and Schrag, 2010; Li et al., 2016; Fantle and Higgins, 2014; Higgins et al., 2018). Consequently, there is increased interest in using Mg isotopes in carbonate records to investigate various geological processes and paleo-environmental changes. Magnesium isotopes in carbonates have been applied to a number of research problems, including chemical weathering and seawater chemistry in the aftermath of the Snowball Earth events (Kasemann et al., 2014; Liu et al., 2014; Huang et al., 2016), hydrothermal and metamorphic processes (Geske et al., 2012; Azmy et al., 2013; Lavoie et al., 2014; Walter et al., 2015), hydro-geochemical processes in karst systems (Buhl et al., 2007; Riechelmann et al., 2012), and formation of "molar tooth" carbonates in Precambrian oceans (Shen et al., 2016). Specifically, the control of carbonate precipitation on seawater chemistry, coupled with the large Mg isotope fractionation during carbonate precipitation, implies a link between global Mg sequestration into carbonate rocks and the Mg isotope composition of seawater. Tipper et al. (2006) first proposed that the Mg isotope composition of seawater is a function of the Mg flux ratio between hydrothermal circulation and carbonate precipitation. This led Li et al. (2015) to propose a calculated δ^{26}Mg curve for seawater through the Phanerozoic, based on the mass balance of Mg between coeval dolomite and hydrothermal fluxes through geological history.

One of the fundamental issues in applications of Mg isotopes in carbonates is the robustness of their primary depositional signatures to post-depositional processes, such as early diagenesis, metamorphism, and hydrothermal alteration. Previous studies have shown that high-Mg calcite and aragonite of marine origin are thermodynamically unstable and have a tendency to transform to low-Mg calcite even at low temperatures (Aissaoui, 1988; Bertram et al., 1991; Bischoff et al., 1993). The behavior of Mg isotopes during these mineral transformations may be complex (Mavromatis et al., 2017b). Hydrothermal alteration experiments have revealed that δ^{26}Mg values of brachiopods and echinoids (both low-Mg calcite) are sensitive to diagenetic alteration (Riechelmann et al., 2016; Riechelmann et al., 2018), even though low-Mg calcite is considered to be more thermodynamic stable. For example, Pogge von Strandmann et al. (2014) and Higgins and Schrag (2015) both measured the Mg isotope compositions of low Mg-calcites in pelagic biogenic carbonates over the Cenozoic. There is, however, considerable inconsistency between these two studies. Relative to calcite, dolomite is significantly more resilient to burial metamorphism in preserving its Mg isotope signatures (Geske et al., 2012; Azmy et al., 2013; Geske et al., 2015a; Hu et al., 2017). However, attempts to reconstruct seawater δ^{26}Mg using dolomite records rely on the assumption that dolomite was in equilibrium with coeval seawater (Li et al., 2015). The high energy barrier of Mg dehydration prevents direct precipitation of dolomite from modern seawater via an abiotic reaction pathway at Earth's surface conditions (Sibley et al., 1987; Arvidson and Mackenzie, 1999), and formation of dolomite occurs in soft sediments in the presence of microbes, or within carbonate rocks via mineral replacement by saline fluids (Katz and Matthews, 1977; McKenzie et al., 1980; Qing et al., 2001; Petrash et al., 2017). Consequently, dolomite is commonly viewed as a diagenetic mineral (Land, 1985; Machel, 2004; Hips et al., 2015).

Early studies of Mg isotopes in dolomites have demonstrated that diagenesis may have different effects on Mg isotope compositions in dolomite (e.g., Geske et al., 2012; Mavromatis et al., 2014). Diffusion–advection–reaction models have been developed in an attempt to understand Mg isotope fractionation during dolomitization within the sediment column (Higgins and Schrag, 2012; Fantle and Higgins, 2014; Blättler et al., 2015; Huang et al., 2015). These numerical models emphasized the importance of diffusion in driving Mg isotope variability in dolomitization profiles. Recently, Higgins et al. (2018) presented a detailed Mg—Ca isotopic study of Neogene and Quaternary shallow marine carbonates. This recent study suggested that in many cases advection dominates over diffusion in controlling the Mg isotope compositions of shallow-water dolomitized carbonates, and thus Mg isotopes in dolomites are often "fluid-buffered". Clearly, more research is needed to comprehensively understand the effects of early diagenesis on Mg isotopes in dolomites, before their successful application to relevant geological problems. In addition, early stage dolomitization is associated with changes in the mineralogical parameters of dolomite in terms of stoichiometry and cation ordering (Rodriguez-Blanco et al., 2015; Kaczmarek and Thornton, 2017), yet the isotopic effects

of the mineralogical changes in dolomite during early diagenesis remain poorly constrained.

Thick, massive, Cretaceous dolomite sequences crop out in the Levant region (Sass and Bein, 1982) in Israel, and contain well-preserved mineralogical and geochemical features clearly related to early diagenesis. Deep burial diagenesis has not affected this section given its local burial history (Bar et al., 2013), and thus these sections provide an excellent opportunity for investigating Mg isotope behavior during early diagenesis. Notably, these dolomite sequences were formed from seawater of the lowest Mg/Ca ratio in the Phanerozoic (Ries, 2006; Coggon et al., 2010), before a steep decrease in the dolomitization intensity on a global scale (Wilkinson and Algen, 1989). In this contribution, we carried out a systematic study on an Early Cretaceous section in central Israel (Judea Mountains), characterized by massive dolomites formed on the Levant carbonate platform. We determined the trace element concentrations and Mg—C—O isotopic compositions of the dolomites, and integrated these data with mineralogical observations, to investigate the impact of early diagenesis on Mg isotopes. A detailed understanding of early diagenetic processes and their effects on Mg isotopes is crucial for future applications of Mg isotopes as an environmental proxy in dolomite.

2. GEOLOGICAL BACKGROUND AND SAMPLES

The study area is located at the Levant margin (Fig. 1), which together with the Levant Basin, are preserved fragments of the Tethys Basin after its closure during the Cenozoic (Gardosh et al., 2010). During the Barremian, the northernmost edge of the Arabian Plate was situated near the equator (Fig. 1A and B; Eppelbaum and Katz, 2011), and hence a favorable site for the accumulation of stable carbonate platform sequences (Ziegler, 2001). These carbonates were deposited in cyclical packages as the southern Tethyan margin experienced rapid and punctuated regressive–transgressive cycles during the Albian (Immenhauser and Scott, 2002).

The Early Cretaceous sequence in this region contains many regional unconformities and lateral facies changes that allow the strata to be subdivided into several groups (Rosenfeld and Hirsch, 2005). In southern Israel, much of the Barremian–Albian interval is represented by marine siliciclastic rocks, whereas this interval in northern Israel is represented mostly by outer shelf carbonates interfingered with slope muds (Bialik and Waldmann, 2017). This first platform sequence after the siliciclastic sequence is mapped as the Judea group (Fig. 1). The platform sequence first formed in the southern Galilee and Coastal Plain regions in the early Albian and extended to the southernmost Negev by the early Cenomanian. In the Judea Mountains, this sequence comprises three formations: Kefira Formation (marl, limestone, and dolomite), Givat Ye'arim Formation (massive dolomite), and Soreq Formation (marl and dolomite). The Early Cretaceous sequence is capped by a thin unit called the Kesalon Formation (limestone and dolomite), which is not always identifiable. Unlike their equivalent in southern Israel (Bialik et al., 2018), these units

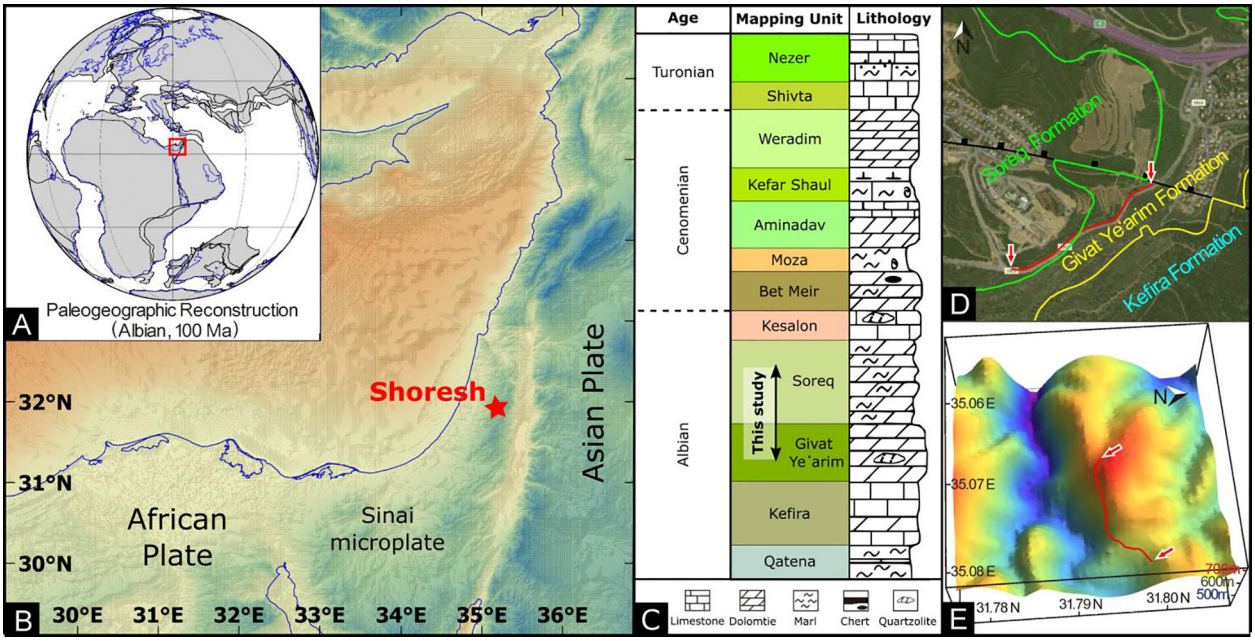

Fig. 1. Geological background of the sampling site. A: Reconstructed global paleogeographic map (source http://www.odsn.de) during the Albian. The southeastern Mediterranean region is marked with red square. B: Shaded relief map of the southeastern Mediterranean. The red star marks the location of the Shoresh section. C. The Albian-Turonian lithostratigraphy of the study area. D: Satellite map of Shoresh Section, with the red line marking the location of the outcrop. The green lines are the strata boundary between the Soreq Formation and Givat Ye'arim Formation, and the yellow line is the strata boundary between the Givat Yearim Formation and Kefira Formation (Modified from the Geological map of Israel 1:50000, Sheet 11-I). E: The 3D topographic map of the Shoresh area, with sampling sites marked with the red line. (For interpretation of the references to colour in this figure legend, the reader is referred to the web version of this article.)

exhibit little evidence of shallow-water facies, apart from the top of the Kesalon Formation that is dominated by calcareous mud-dominated facies when not dolomitized (Sass and Bein, 1982).

In the Shoresh section near Jerusalem (Fig. 1C and D), the Givat Ye'arim and Soreq formations are well exposed (Fig. 2A). The overlying Soreq Formation consists of argillaceous dolomites, uniformly and well-bedded (0.5–1.0 m thick) soft dolomite, and interbedded marl, whereas coarsely to medium crystalline thickly bedded dolomites are present in the Givat Ye'arim Formation (Arkin et al., 1965). Limestone dominates the Kefira Formation that underlies the Givat Ye'arim Formation in the Shoresh section. These rock units have experienced little deformation and retain near-horizontal bedding. Systematic sampling of the lower part of the Soreq Formation

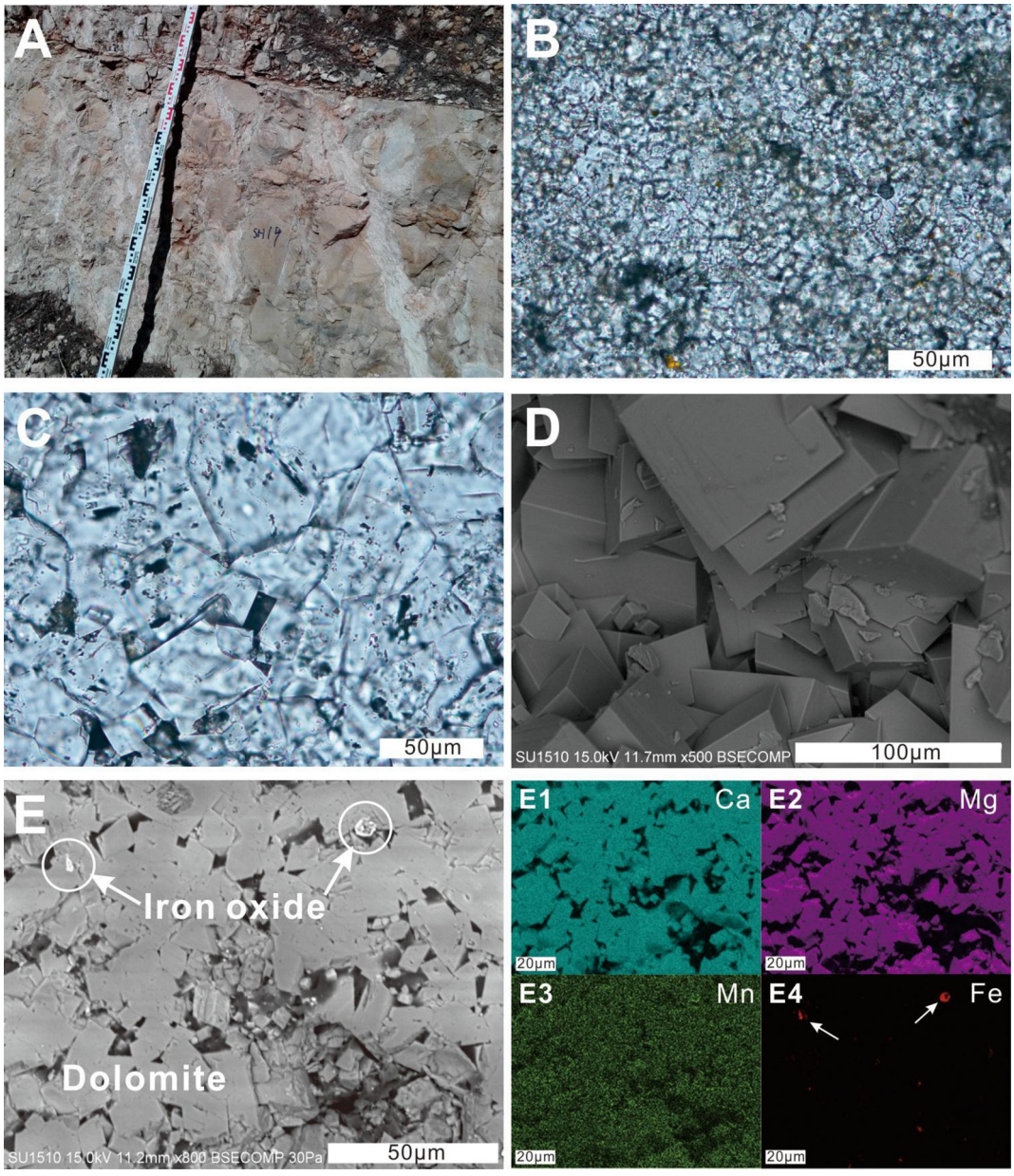

Fig. 2. Images showing the characteristics of the Shoresh dolomites. A: Thick dolomite layers in the outcrop. B: Euhedral dolomite with crystal size between 10–20 μm (SU-07, Soreq Formation). C: Subhedral to euhedral dolomite with crystal size over 50 μm (SH-12, Givat Ye'arim Formation). D: Euhedral rhombohedra dolomite crystals (BSE, SH-30, Givat Ye'arim Formation). E: Back scatter image and elemental mapping (E1–E4) of a Mn-rich dolomite sample (SU-15, Soreq Formation), arrows denote Fe oxides, note the even distribution of Ca, Mg, and Mn in the dolomite and the uneven distribution of Fe as iron oxides.

through to the upper part of the Givat Ye'arim Formation was undertaken, and 53 samples were collected over a stratigraphic thickness of 83 m (Fig. 1C and D).

3. ANALYTICAL METHODS

3.1. Petrographic and mineralogical analyses

Thin-sections were prepared of all samples for optical microscopy and scanning electron microscopy (SEM) observations. SEM images were taken using a Hitachi SU1510 scanning electron microscope at the School of Earth Sciences and Engineering, Nanjing University, China. The mineralogy of the samples was analyzed using a Rigaku RAPID II X-ray diffractometer at the State Key Laboratory for Mineral Deposits Research, Nanjing University, China, using a rotating Mo anode X-ray source operated at 50 kV and 90 mA. The X-ray diffraction pattern for the powdered rock sample was collected using a two-dimensional image plate, and a 10 min exposure time was used for each analysis. Data reduction and interpretation were performed using a combination of Rigaku 2DP and PDXL software and Jade 6.5 software. The relative abundance of calcite and dolomite in each sample was calculated based on the peak intensity of (104) for the two minerals (Royse et al., 1971). Stoichiometry of dolomite or calcite was calculated based on the $d(104)$ value according to Goldsmith and Graf (1958). The degree of order of dolomite was calculated following the equation of Graf and Goldsmith (1956): $R = I(015)/I(110)$, where I is the intensity of the (015) or (110) peaks.

3.2. Elemental analysis

Approximately 50 mg of rock powder was digested in 4 mL of 7 M HCl. The dissolved sample (supernatant) was transferred into a new Teflon beaker, then transformed to nitrates by repeatedly drying in concentrated HNO_3, and was subsequently diluted into 50 mL of 2% HNO_3. Elemental concentrations were analyzed using an Aurora M90 quadrupole inductively coupled plasma–mass spectrometer (ICP–MS) at the State Key Laboratory for Mineral Deposits Research, Nanjing University, China. The ICP–MS analyses were undertaken in standard operating conditions, and a series of gravimetrically prepared multi-element solutions were used as external standards. A dolomite standard material (GSR-12) from the Ministry of Land and Resources of China was analyzed after every 10 sample analyses for data quality control. The analytical precision was <10% (RSD in %) for most elements.

3.3. Carbon and oxygen isotope analysis

Carbon and O isotopes were measured by Thermo Finnigan Delta V Plus continuous flow isotope ratio mass spectrometry (IRMS) at the State Key Laboratory for Mineral Deposits Research, Nanjing University, China. Approximately 80–120 μg of carbonate powder was reacted with orthophosphoric acid for >12 h at 70 °C in a continuous flow sample preparation device Gas Bench II that is connected to the IRMS. Chinese GBW00405 carbonate standards TTB-1 (calcite) and TTB-2 (dolomite) were analyzed for two-point isotope ratio normalization according to Paul et al. (2007). Both the C and O isotope ratios were normalized to Vienna PDB in δ notation. Internal precision was better than ±0.09‰ (1SD) for $\delta^{13}C$ and ±0.08‰ (1SD) for $\delta^{18}O$, and the external reproducibility was better than ±0.5‰ for both $\delta^{13}C$ and $\delta^{18}O$ values.

3.4. Mg isotope analysis

Based on the elemental analysis results, an aliquot of dissolved sample that contained ~100 μg of Mg was used for Mg isotope analysis. Magnesium was purified following a two-stage ion exchange procedure that has been detailed by Hu et al. (2017). Briefly, the sample was first dissolved in 0.5 mL of 1.5 M HNO_3 and loaded on a custom-made quartz column filled with 1 mL of AG 50 W-X12 (100–200 mesh) resin, and eluted with 1.5 M HNO_3 to remove the majority of the matrix elements from Mg. A custom-made PFA column that contained 0.4 mL of AG 50 W-X8 (100–200 mesh) resin was used for further purification of Mg. In the second column procedure, the sample was dissolved in 0.5 mL of mixed acid (0.2 M HNO_3 and 0.05 M HF) and loaded onto the resin. The column was eluted sequentially using different acids that further separated Ti, K, Na, and Ca from Mg (Hu et al., 2017). All of the chemical procedures were performed in a Class 100 fume hood in a Class 1000 clean room. All labware was acid-washed before usage, and double-distilled acid and deionized water (>18.2 MΩ) were used throughout the experiments. Recovery of Mg was better than 98%, and the total procedural blank was <80 ng, which is <0.1% of the total Mg in each sample and therefore negligible.

Magnesium isotope ratios were measured using a Thermo Scientific NEPTUNE Plus multi-collector MC-ICP-MS at the State Key Laboratory for Mineral Deposits Research, Nanjing University, China. The instrument was operated in a standard wet plasma, low resolution mode, with a solution uptake rate of 100 μL/min. Standard–sample–standard bracketing was used for the instrumental mass bias correction and the concentration of standard Mg solutions was 1.2 ppm. A pure Mg stock solution (HPS909104) from High Purity Standards Inc. was used as an in-house bracketing Mg standard (Li et al., 2012; Li et al., 2015). The sample concentration typically matched the in-house standard to better than ±10%. A 40 s on-peak acid blank was measured before each analysis. Each Mg isotope ratio measurement consisted of 50 × 4 s integrations, and the typical internal precision (2standard error or 2SE) was better than ±0.04‰ for $^{26}Mg/^{24}Mg$ and ±0.02‰ for $^{25}Mg/^{24}Mg$. Analytical accuracy was assessed by analysis of the international Mg isotope standards DSM3 and Cambridge1. In addition, USGS igneous rock standard materials and seawater were treated as unknown samples and analyzed. Magnesium isotope ratios are reported in δ notation as $\delta^{26,25}Mg = [(^{26,25}Mg/^{24}Mg_{sample})/(^{26,25}Mg/^{24}Mg_{DSM3}) - 1] \times 1000$ relative to the international Mg isotope standard DSM3. The $\delta^{26}Mg$ value of the pure Mg solution HPS909104 relative to DSM3 has been well

calibrated using three different types of MC–ICP–MS at the University of Wisconsin-Madison and Nanjing University for over five years ($\delta^{26}Mg_{HPS} = -0.66‰$ relative to DSM3; Li et al., 2012, 2015; Hu et al., 2017). Based on repeat analyses of multiple geological standards and Mg standard solutions, the long-term external reproducibility is better than ±0.1‰ for $\delta^{26}Mg$.

4. RESULTS

4.1. Petrography and mineralogy

The bulk carbonates are composed predominantly of subhedral to euhedral, finely crystalline dolomite, and SEM and optical microscopy measurements revealed a crystal size range of 10–90 μm (Fig. 2B and C; Table S1). The Soreq Formation is characterized by smaller crystals (average = 19 μm; 1SD = 7 μm; n = 24) relative to the underlying Givat Ye'arim Formation (average = 42 μm; 1SD = 21 μm; n = 28). Most of the rock samples contain variable degrees of porosity in the form of cavities and pores, where the size of individual dolomite crystals can reach 100 μm (Fig. 2B–D; Table S1).

X-ray diffraction analyses indicated that the samples are composed mostly of pure dolomite. Based on the stoichiometry of dolomite calculated from *d*(104) values, dolomite can be divided into three distinct groups: near stoichiometric dolomite [$Ca_{1.00–0.96}Mg_{1.00–1.04}(CO_3)_2$], magnesian dolomite [$Ca_{0.93}Mg_{1.07}(CO_3)_2$], and calcic dolomite [$Ca_{1.04–1.03}Mg_{0.96–0.97}(CO_3)_2$] (Table S1). Dolomite stoichiometry varies through the stratigraphic section (Fig. 3), whereby calcic dolomite dominates in the lower part of the section in the Givat Ye'arim Formation, near stoichiometric dolomite dominates the middle to upper part of the section, and magnesian dolomite is found in the upper part of Givat Ye'arim and Soreq formations.

Magnesian, near stoichiometric, and calcic dolomite are characterized by decreasing cation ordering *I*(015/110) values that have averages of 0.526, 0.469, and 0.337, respectively (Fig. 3; Table S1). Dolomite from the upper part of the section has lower *d*(104) values and higher cation ordering than dolomite from the lower part (Fig. 3). The full-width-at-half-maximum (FWHM) of the dolomite (104) peak is also greater in the lower part of the section (Fig. 3).

4.2. Trace elements

Manganese contents of the bulk carbonates range from 71 to 707 ppm throughout the section, and a prominent excursion to high Mn occurs in the middle of the Soreq Formation. It should be noted that no Mn oxide minerals were identified in the high Mn samples. However, energy dispersive X-ray spectroscopy (SEM-EDS) mapping of the high-Mn dolomite samples indicates that Mn is distributed uniformly in the dolomite crystals, indicating lattice substitution by Mn (Fig. 2E).

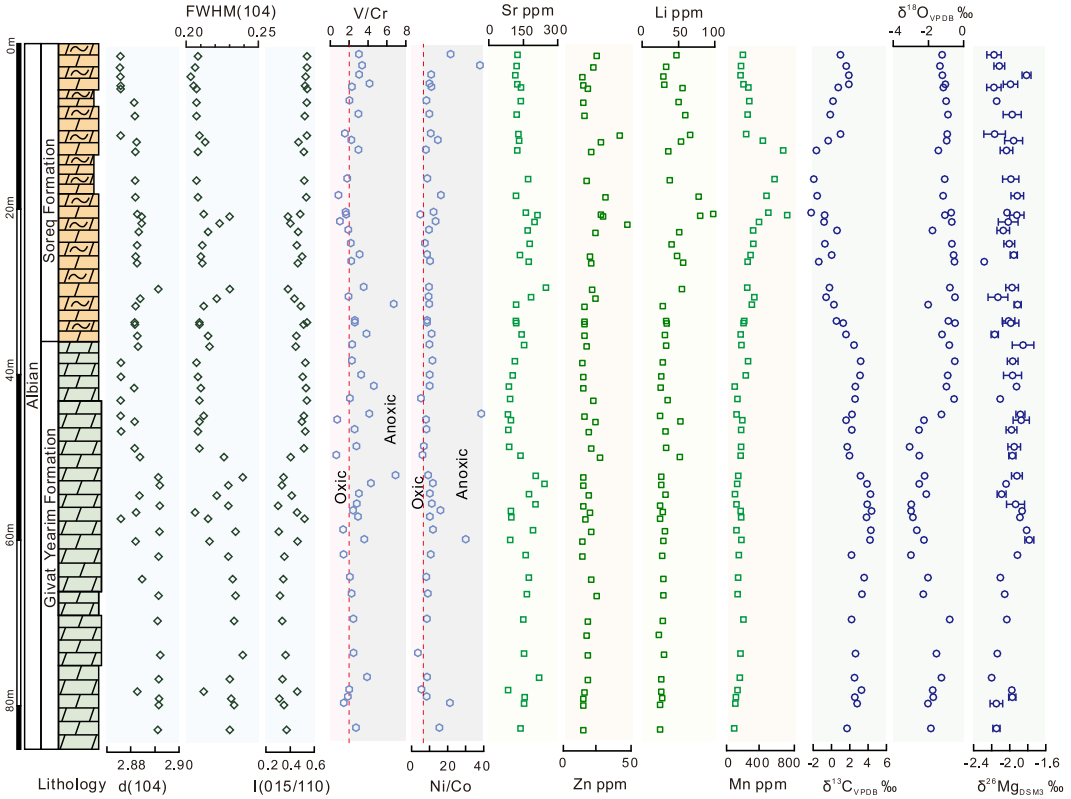

Fig. 3. Variation of lithology, mineralogical parameters, redox-sensitive elemental ratios, bulk rock elemental concentrations and C—O—Mg isotope compositions of dolostone samples from the Shoresh section.

Strontium contents of most samples vary from 100 to 250 ppm (Fig. 3), except for several samples that contain anomalously high Sr (Table S2). Strontium concentrations decrease with increasing degree of dolomite ordering (Fig. 4A). V/Cr and Ni/Co ratios (ppm/ppm) range from 0.6 to 7.1 and 3.7 to 38.9, respectively, and most samples have V/Cr > 2 and Ni/Co > 7 (Fig. 3). Elevated Li, Ti, and Zn contents are evident in the upper part of the section (Table S2).

4.3. Isotopic compositions

Bulk carbonate samples in the Shoresh section have $\delta^{13}C_{V\text{-}PDB}$ values of −2.17‰ to 4.47‰ and $\delta^{18}O_{V\text{-}PDB}$ values of −3.03‰ to −0.08‰ (Table S3). These values are consistent with those reported by Sass and Katz (1982). $\delta^{13}C$ values of dolomite from the Givat Ye'arim Formation are comparable with the Albian carbonate $\delta^{13}C$ record from Katz et al. (2005). However, the more negative $\delta^{13}C$ values from the upper Soreq Formation have rarely been reported in contemporaneous carbonate records (e.g., Li et al., 2016). $\delta^{18}O$ values of dolomites are slightly higher than the tropical to subtropical planktonic foraminifera $\delta^{18}O$ records of the Albian interval (Grossman, 2012). The lowest $\delta^{18}O$ value occurs in the upper part of the Givat Ye'arim Formation. The Givat Ye'arim Formation has relatively positive $\delta^{13}C$ values compared with the Soreq Formation and, in the middle of the Soreq Formation, the $\delta^{13}C$ data exhibit a prominent negative excursion down to −2.17‰, which is coincident with the positive excursion in Mn contents (Fig. 3), as well as Li and Zn contents. $\delta^{13}C$ values show a negative correlation with Mn concentrations in bulk samples (Fig. 4B). Dolomite $\delta^{18}O$ values exhibit a general negative correlation with $\delta^{13}C$ values (Fig. 4C).

Bulk rock $\delta^{26}Mg$ values range from −2.28‰ to −1.78‰ (Table S3), with an average value of −2.01‰ ± 0.22‰ (2SD; n = 53), which is consistent with the $\delta^{26}Mg$ values of dolostones (−2.29‰ ± 0.10‰ and −2.30‰ to −1.52‰) from the coeval strata reported by Galy et al. (2002) and Bialik et al. (2018), respectively. Despite the variation in $\delta^{26}Mg$ values in the samples that is analytically resolvable, there is no noticeable trend in $\delta^{26}Mg$ through the strati-

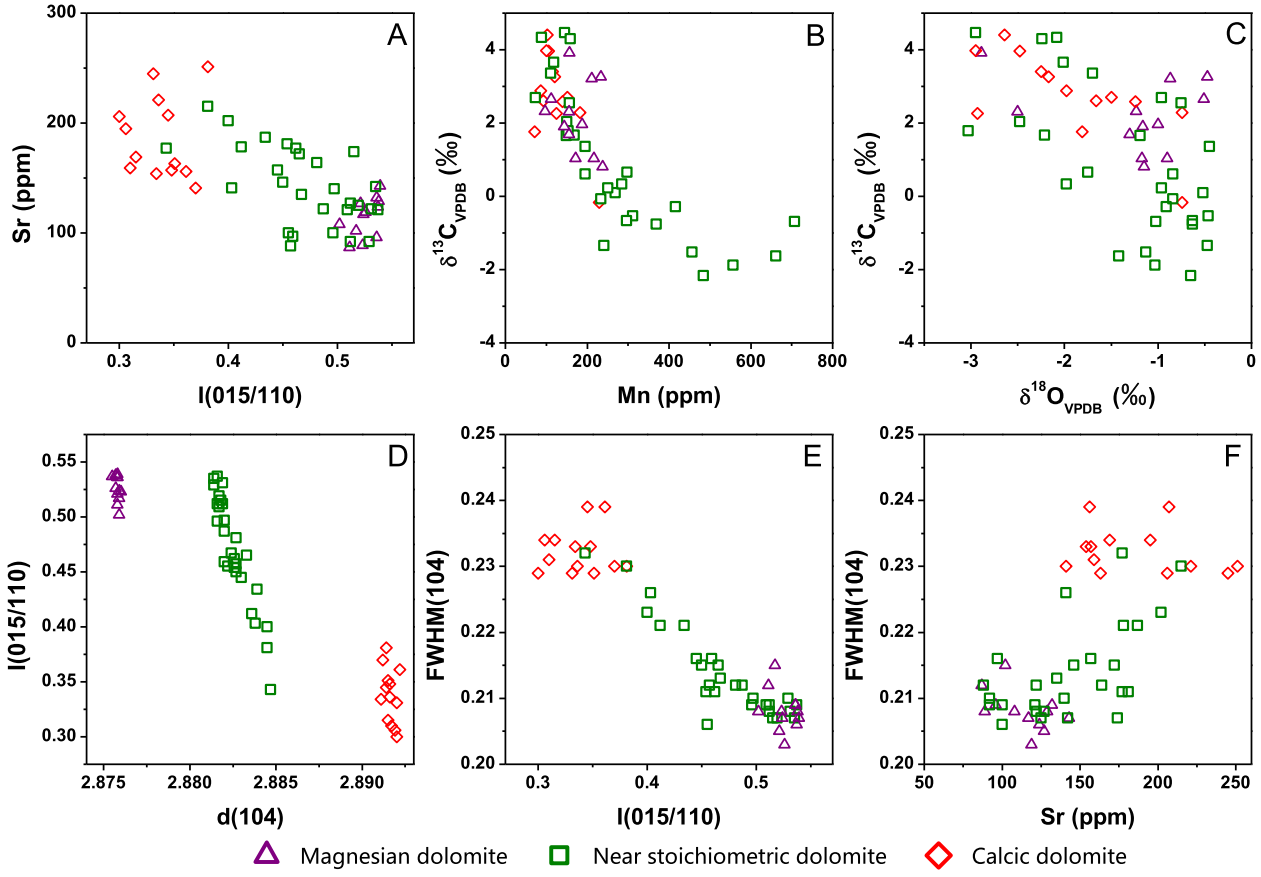

Fig. 4. Cross-plots of dolomite mineralogical parameters, Sr and Mn abundances, and C—O isotopic compositions. Diamond, square and triangle symbols stand for calcic dolomite, near stoichiometric dolomite and magnesian dolomite respectively. a: Negative correlation between dolomite Mn contents and $\delta^{13}C$ values. b: Negative correlation between Sr concentration and degree of dolomite ordering I(015/110). c: A weak negative correlation between dolomite $\delta^{13}C$ and $\delta^{18}O$ values. d: Distinctive Dolomite crystallographic degree I(015/110) decreases with increased *d*(104) value. e: Negative correlation between dolomite cation ordering I(015/110) and FWHM of (104) peak. f: Positive correlation between dolomite Sr concentration and FWHM of (104) peak (see Appendix A, Table S5 for statistical parameters).

graphic section (Fig. 3). $\delta^{26}Mg$ does not correlate with any other geochemical or mineralogical parameters examined in this study, including $\delta^{13}C$ values, *d* values and FWHMs of the dolomite (104) peak, degree of dolomite cation ordering, and Sr and Mn concentrations (Fig. 5). There is no clear correlation ($R^2 = 0.1$) between $\delta^{26}Mg$ and $\delta^{18}O$ of dolomite, either, although dolomite with the lowest $\delta^{26}Mg$ values tends to have $\delta^{18}O$ close to 0‰.

5. DISCUSSION

The Albian dolostones from the Shoresh area are regarded as the product of early diagenetic (penecontemporaneous) dolomitization within soft sediment, which has preserved the original mineralogy and chemistry since their formation (Sass and Bein, 1982; Sass and Katz, 1982). Dolomite throughout the section displays an idiotopic texture (i.e., euhedral to subhedral crystals with straight, inter-crystal boundaries; Fig. 2B–D), which is indicative of mineral precipitation below the critical roughening temperature of 50 °C (Gregg and Sibley, 1984), supporting an early diagenetic origin. There are marked variations in mineralogy and geochemistry, which contain clues to deciphering the effects of diagenesis on Mg isotopes in dolomites.

5.1. Precipitation of dolomite in the Mn(IV)-reduction zone and the Mg isotope response

Based on the paleo-redox indices of V/Cr and Ni/Co ratios (Bryn Jones, 1994), the high V/Cr and Ni/Co ratios of the dolomite in the Shoresh section indicate that the dolomite was precipitated in a predominantly suboxic environment (Fig. 3), probably within soft sediment. The decreasing trend of $\delta^{13}C$ values in the Soreq Formation implies an increase in contribution of isotopically light carbon that was sourced from organic matter degradation within the sediment. Notably, dolostones from the upper Soreq Formation contain elevated Mn concentrations that negatively correlate with $\delta^{13}C$ values (Figs. 3 and 4B). Due to the higher free energy yield, MnO_2 of detrital origin could be an effective oxidant and is more efficient in producing alkalinity through the Mn(IV) reduction reaction (i.e., $CH_3COO^- + 4MnO_2 + 3H_2O \rightarrow 4Mn^{2+} + 2HCO_3^- + 7OH^-$) than the bacterial sulfate reduction pathway under anoxic and organic-rich conditions (Petrash et al., 2015; Petrash et al., 2017). The reduced form of Mn(II) is readily incorporated into carbonate lattices (Barnaby and Rimstidt, 1989), consistent with the SEM-EDS mapping of the high Mn dolomite samples (Fig. 2E). Previous research has also implied that Mn cycling could have an

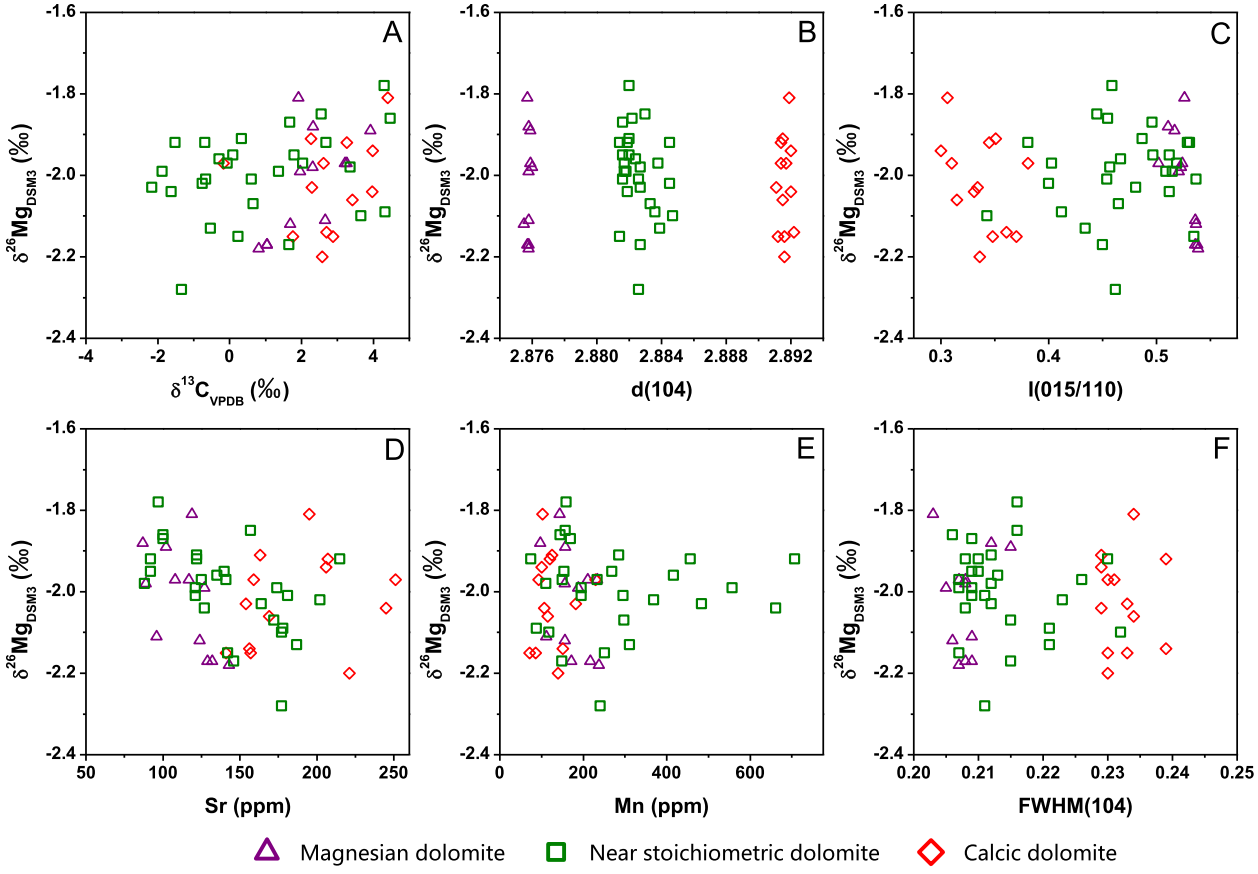

Fig. 5. Plots of dolomite $\delta^{26}Mg$ values versus other geochemical and mineralogical parameters. Diamond, square and triangle symbols stand for calcic dolomite, near stoichiometric dolomite and magnesian dolomite respectively (see Appendix A, Table S5 for statistical parameters).

important role during early diagenetic dolomite formation (Petrash et al., 2015; Petrash et al., 2017). Degradation of organic matter results in enrichment of light C isotopes in dissolved inorganic carbon (DIC) in pore water, and the accumulation of this promotes carbonate precipitation and leads to lower $\delta^{13}C$ signatures in the carbonates.

It should be noted that Li and Zn concentrations also increase in this low $\delta^{13}C$ and high Mn interval (Fig. 3). Given that Li is a proxy for continental inputs (Wedepohl, 1995) and Zn is a micronutrient element for organisms (Morel et al., 1994), the increase in Li and Zn contents implies a period of higher primary productivity boosted by an increased nutrient supply from continental runoff. In an epicontinental basin setting such as our study site, an increase in primary productivity would enhance organic carbon burial. Due to the mineralization of organic matter, reduction of MnO_2 and incorporation of Mn^{2+} into the dolomite lattice must have occurred in soft sediments prior to lithification of the carbonates. As such, the correlation between $\delta^{13}C$ values and Mn contents ($r = -0.70$; $p \ll 0.01$) places a strong constraint on the early diagenesis origin of the dolomite investigated in this study.

In the presence of organic matter in soft sediments, micro-organisms utilize a series of respiratory pathways for metabolism, which are, downward from the sediment–seawater interface, aerobic respiration, denitrification, manganese oxide reduction, iron oxide reduction, sulfate reduction, anaerobic oxidation of methane, and methanogenesis (Fig. 6). Manganese oxide reduction occurs in shallower zones of soft sediments than iron reduction, sulfate reduction, and methanogenesis (Froelich et al., 1979; Canfield et al., 1993; D'Hondt et al., 2004). It has been reported that the Mn(IV) reduction zone in platform sediments can be as shallow as a few centimeters to a few tens of centimeters below the sediment–water interface (Burdige, 1993; Canfield et al., 1993; Thamdrup et al., 1994). The continuity of dolomite deposition and uniformity of the dolostone layers in the Shoresh section implies that the dolostones in both the Givat Ye'arim and Soreq formations were formed in shallow sediments around the Mn(IV) reduction zone.

During diagenesis, dolomite precipitation via different pathways may have different Mg—C isotopic responses. Mavromatis et al. (2014) reported two types of dolomite from deep-sea sediments at the Peru margin. One type is associated with near-seafloor anaerobic methane oxidation and the other is from the deeper methanogenesis zone. The two types of dolomite show distinct $\delta^{26}Mg$ and $\delta^{13}C$ signatures, reflecting differences in Mg supply and reaction mechanisms for producing alkalinity. Similarly, Blättler et al. (2015) studied authigenic dolomite from the Miocene Monterey Formation and found very large variations in both $\delta^{13}C$ and $\delta^{26}Mg$ values of dolomite, which were interpreted to reflect dolomite precipitation under limited Mg supply in zones of bacterial sulfate reduction or methanogenesis (Fig. 7). In contrast, Fantle and Higgins (2014) and Higgins et al. (2018) reported that dolomites from carbonate platforms have a narrow range of $\delta^{26}Mg$ values, and suggested that dolomite precipitation was buffered by advecting seawater, and not limited by Mg transport via

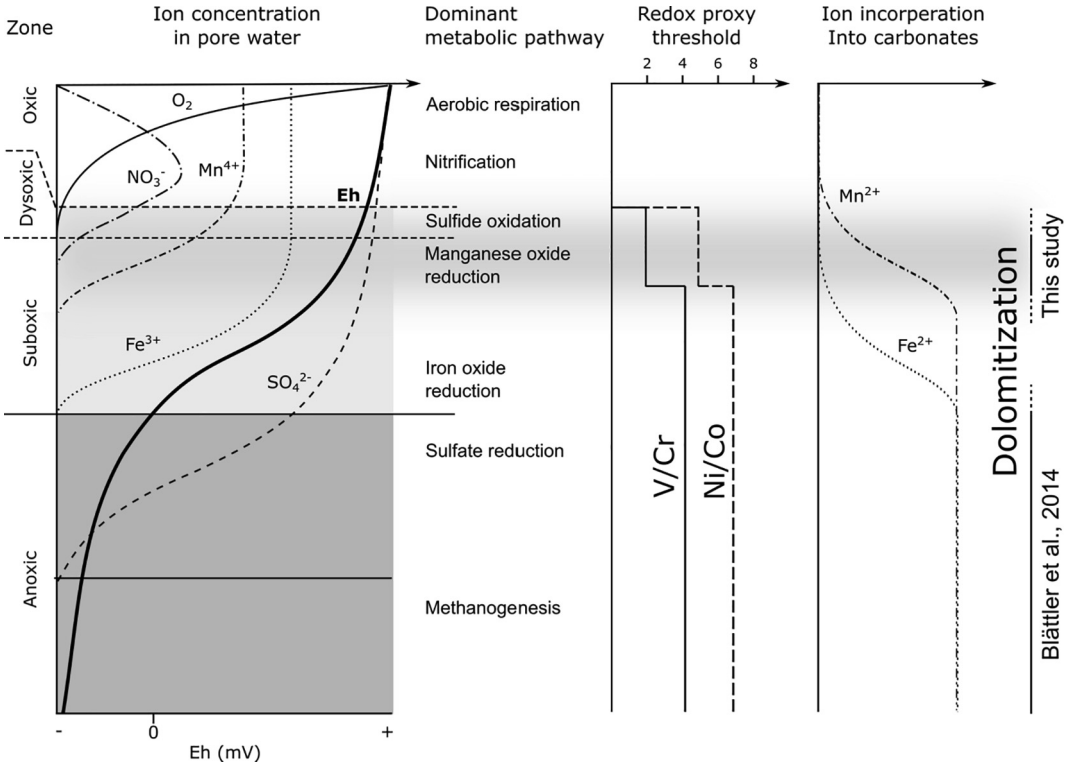

Fig. 6. A vertical profile of electron acceptor availability, Eh, and microbial metabolism across a depth/redox gradient in soft sediment, and co-variation in paleo-redox proxies and ion speciation of Mn and Fe. Modified after Petrash et al. (2017).

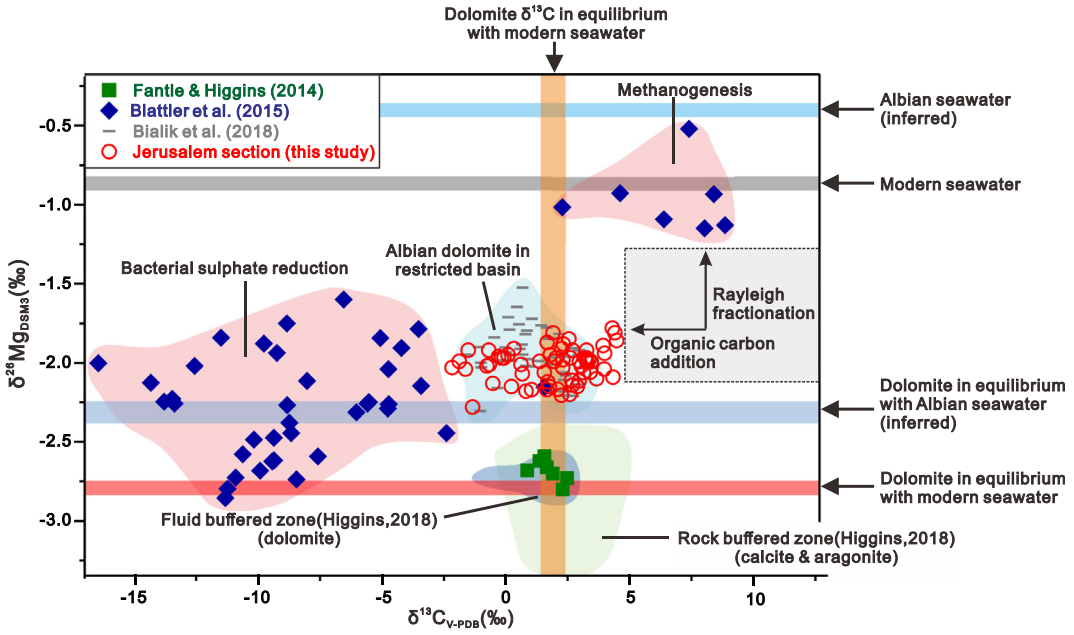

Fig. 7. Cross plot of $\delta^{13}C$ versus $\delta^{26}Mg$ for dolomite from different settings and ages. Note that Higgins et al. (2018) reported a large dataset for many marine carbonate sediments, and because of the large size of the data, only the fields of the data plots are marked for clarity.

diffusion (Fig. 7). Modeling work by Ahm et al. (2018) suggested that on advective timescales, Mg sequestering rates are not sufficient to result in a significant removal of Mg from each parcel of water to develop notable isotopic effects from Rayleigh distillation. In this study, dolostones from the Shoresh section formed in a carbonate platform setting (Sass and Bein, 1982) also have a narrow range of $\delta^{26}Mg$ values ($-2.01‰ \pm 0.22‰$; 2SD; n = 53), which implies that Mg isotopes in the dolomites were likely "fluid-buffered", similar to the cases reported by Fantle and Higgins (2014) and Higgins et al. (2018). More importantly, geochemical signatures ($\delta^{13}C$ values and Mn contents) indicate that the dolomite was formed in the shallow MnO_2 reduction zone, which was predominantly influenced by seawater advection and much less prone to Mg supply limitation than the deeper zones of bacterial sulfate reduction and methanogenesis (Fig. 7).

The influence of seawater on the isotopic signature of dolomite from the Shoresh section can be estimated based on isotopic and elemental mass balance considerations. Organic matter typically has $\delta^{13}C$ values that are more than 20‰ lower than dissolved inorganic carbon (DIC) in seawater (Farquhar et al., 1989), yet the low $\delta^{13}C$ values of the Soreq Formation are just slightly below 0‰ (−2‰; Fig. 3). As such, the contribution of low $\delta^{13}C$ DIC from MnO_2-reduction is small relative to the DIC from seawater. Assuming that the DIC of seawater that was advecting in soft sediments during precipitation of dolomite in the Shoresh section had a $\delta^{13}C$ value of 0‰, a simple isotopic mass balance calculation requires that low $\delta^{13}C$ organic carbon contributed to <10% of the carbonate in the dolomite lattice, and that the pore water was dominated by DIC from seawater during dolomite precipitation. This implies that the dolostones were formed in soft sediments close to the seawater–sediment interface. We note that although the contribution of organic carbon is small, its isotopic signature is still recognizable (i.e., Fig. 4B). However, seawater has a high Mg:C molar ratio (e.g., $Mg:HCO_3^- = 27.5$ for modern seawater; (Demicco et al., 2005), and thus Mg isotopes in dolomite from the MnO_2 reduction zone must have been buffered by seawater. Therefore, the lack of a correlation between $\delta^{26}Mg$ and $\delta^{13}C$ values in dolomite in this study (Fig. 5A) reflects a combined effect of the shallow depth of dolomite formation during MnO_2 reduction and the high Mg:C molar ratio of seawater, which resulted in a high fluid/rock ratio for Mg but a lower fluid/rock ratio for C during advection of seawater in soft sediments.

5.2. Recrystallization of dolomite and the Mg isotope response

Experimental studies suggest that well-ordered dolomite forms from metastable precursors of disordered proto-dolomite via recrystallization (Kaczmarek et al., 2014). The relative intensity of super-lattice X-ray reflection *I* (015/110) is an indicator for cation ordering in dolomite (Goldsmith and Graf, 1958). Within the dataset presented here, there is a negative correlation ($R^2 = 0.83$; n = 53) between the *d*(104) value ($MgCO_3$ content) and *I* (015/110). The calcic dolomite is generally less ordered, whereas magnesian dolomite has a higher degree of cation ordering, and the degree of order for near-stoichiometric dolomite is intermediate (Fig. 4B). Moreover, the negative correlation between *d*(104) and *I*(015/110) exists for each of the three dolomite subgroups. This negative correlation between *d*(104) and *I*(015/110) was also observed in experimental dolomite synthesis studies (Li et al., 2015; Kaczmarek and Thornton, 2017), and was interpreted to

reflect ripening towards higher crystallinity. Indeed, the FWHM of the dolomite (104) peak, which is a parameter of mineral crystallinity (Demény et al., 2016), is negatively correlated with I(015/110) (Fig. 4E). The exact reason for higher cation ordering in low d(104) (or high-Mg) dolomite has not been discussed in literature, and will be an interesting topic for future researches.

Diagenetic processes also had an impact on dolomite Sr contents. As the cation ordering of dolomite increases, the Sr concentration decreases (Fig. 4A), reflecting Sr loss during recrystallization of dolomite. Given that Sr^{2+} has a larger ionic radii than Ca^{2+} (Shannon, 1976), ordering of dolomite would result in exclusion of Sr from the mineral lattice (Land, 1985; Vahrenkamp and Swart, 1990), generating the observed negative correlation between cation ordering and Sr contents (Fig. 4A). Recrystallization would also increase the crystallinity of the dolomite mineral, decreasing the FWHM of the dolomite (104) peak (i.e., making X-ray diffraction peaks sharper; Fig. 4F). Therefore, variations and correlations between dolomite lattice parameters (cation ordering and X-ray diffraction peak sharpness) and Sr contents are also indicative of variable degrees of crystallization during diagenesis of dolomite.

X-ray diffraction data (i.e., d(104) values) reveal that there is a significant compositional variability in dolomite stoichiometry in the analyzed samples. According to *ab initio* calculations by Wang et al. (2017), the equilibrium fractionation of Mg isotopes in carbonates is a function of the Mg/Ca ratio, or the average Mg—O bond lengths of carbonate, and the equilibrium Mg isotope fractionation factor changes by 0.2‰ at 300 K when dolomite Mg/(Mg + Ca) ratios changes from 0.48 to 0.54, a range displayed by the dolomites from the Shoresh section. The hydrothermal synthesis experiments for dolomite by Li et al. (2015) also showed that the $\Delta^{26}Mg_{dol-aq}$ fractionation factor for poorly ordered dolomite is lower than that of ordered dolomite at the same temperature. Li et al. (2015) reported that recrystallization of dolomite was accompanied by systematic changes in d(104) values and I(015/110) ratios, and interpreted it to reflect Mg—O bonding effects on Mg isotope fractionation. Therefore, based on previous theoretical and experimental work, some form of correlation between $\delta^{26}Mg$ and d(104) values would be expected in natural dolomites. However, there is no correlation between $\delta^{26}Mg$ and d(104) values of dolomite from the Shoresh section (Fig. 5B; $R^2 = 0.01$; χ/DOF = 0.01; n = 53). The explanation for this is that the dolostones experienced variable degrees of recrystallization in a relatively closed system with a high rock/water ratio that limited isotopic resetting. Indeed, variations in I(015/110), Sr contents, and FWHMs of dolomite imply that the samples underwent different degrees of recrystallization (Fig. 4A, E, F). Given that recrystallization is a prolonged process that may have occurred during early diagenesis and any period of time thereafter, multiple factors may have contributed to the localized variations in the degree of recrystallization.

Following precipitation of dolomite in the shallow soft sediments (i.e., MnO_2 reduction zone), cementation and compaction during early burial would expel pore fluids and decrease porosity, which increasingly limited the interaction between dolomite and the overlying seawater. Eventually, Mg isotopes in the pore fluids changed from predominantly seawater-buffered (i.e., Higgins et al., 2018) to rock-buffered (specifically, dolostone buffered), although recrystallization of dolomite may have continued. In this scenario, Mg contents in pore fluids were not sufficient to change the isotopic composition of bulk dolomite as the pore fluids became increasingly isolated from seawater. Therefore, mineralogical and trace element changes during dolomite recrystallization can vary significantly due to variations in element availability (e.g., Mn^{2+}) and mineralogy-dependent partition behavior (e.g., Sr^{2+}), whilst Mg isotopes behave conservatively. Limited seawater Mg supply in pores relative to the mass of Mg in dolomite in sediments during burial can thus explain the lack of correlation between $\delta^{26}Mg$ values and diagenetic recrystallization parameters (e.g., I(015/110), Sr and Mn contents, and FWHM; Fig. 5C–F). In light of this, conversion from less ordered Ca-dolomite to more ordered Mg-dolomite would be better explained by loss of Ca, rather than gain of Mg, during diagenetic recrystallization of dolomite. Similar conclusions regarding the conservative behavior of Mg isotopes in massive dolostones were made by Geske et al. (2012) and Hu et al. (2017). In contrast, recrystallization results in significant modification of Mg isotopes in calcite (Chanda and Fantle, 2017), which contain less Mg than dolomite.

5.3. Geological implications

Based on the previous discussion, dolomites from the Shoresh section were precipitated at shallow depths below the sediment–water interface, where MnO_2 reduction occurred (Fig. 6). Previous studies (Burdige, 1993; Thamdrup et al., 1994) have shown that the MnO_2 reduction zone can be sufficiently shallow to be well exchanged with seawater above the sediment. Thus, Mg isotopes in the original dolomite in the soft sediments were buffered by contemporary seawater in the sedimentary basin. However, recrystallization occurred in the protracted post-depositional period (i.e., the burial period), when Mg in pore waters and pore water mobility was insufficient to change the Mg isotope composition of the existing dolomite. Notably, a negative correlation between $\delta^{13}C$ values and the carbonate-assimilated Mn contents of dolomite is a unique indicator of Mn(IV) reduction in shallow sediments that can be used to distinguish dolomites formed during bacterial sulfate reduction and methanogenesis. The correlations between $\delta^{13}C$, Mn, Zn, and Li signatures and the >20 m thickness of the interval with such signatures suggest an event in the carbonate platform during deposition, rather than the randomness or heterogeneity within the sediment. Identification of such a signature is critical for using dolomite as a chemical archive of seawater, because dolomite formed in zones of bacterial sulfate reduction and methanogenesis would have modified Mg isotope signatures due to isotopic fractionation associated with diffusion and Rayleigh-type processes in a diffusive regime. These observations in an ancient carbonate platform setting corroborate previous studies that suggested dolomite from carbonate platforms can be buffered by seawater in terms

of Mg isotopes (Fantle and Higgins, 2014; Higgins et al., 2018). However, it should be noted that the dolomite samples still have a variation of 0.4‰ in δ^{26}Mg values, which is several times greater than the external analytical reproducibility. Contemporary seawater has relatively invariant δ^{26}Mg values given the long residence time of Mg in the oceans. Therefore, the variation in δ^{26}Mg values of our dolomite samples reflects some specific process(es) that introduced variability as compared with an open ocean seawater-buffered Mg isotope signature.

Given that the dolostones from the Shoresh section were formed in a microbial-modified environment, interaction of Mg with organic molecules might affect Mg hydration, speciation, effective concentration, and possibly isotopic fractionation. Theoretical studies (Schott et al., 2016) and experimental investigations (Mavromatis et al., 2017a) both show that organic ligands can exert a significant effect on Mg isotope fractionation factors between aqueous solutions and minerals. However, such effects are challenging to evaluate in old sedimentary rocks. In natural systems, the nature of organic ligands might be changed by changes in microbial communities in response to redox variations in the sediment column. In this case, one would expect some correlation between δ^{26}Mg values and Mn contents, but such a correlation is not observed (Fig. 5E). Changes in the abundance of organic matter might also change the speciation of Mg, affecting isotopic fractionation. In this case, one would also expect some correlation between δ^{26}Mg and δ^{13}C values, but such a correlation is not observed (Fig. 5A). In summary, there is no clear evidence that organic matter is responsible for the δ^{26}Mg variations in the dolostones.

An alternative possibility is that the Mg isotope variability results from the inherited isotopic signatures of precursor minerals, if the dolomite formed via a replacement pathway. During the Albian, low-Mg calcite was expected to be the dominant $CaCO_3$ mineralogy, because the ocean had a "calcite sea" chemistry (Dickson, 2002). However, Fantle and Higgins (2014) showed that during dolomitization of calcite, the original δ^{26}Mg signature is rapidly erased, implying that the observed variation in δ^{26}Mg was not caused by the mineral precursors to dolomite. In addition, Higgins et al. (2018) showed that dolomitization of carbonate precursors (calcite and aragonite) is accompanied by an increase in Mg/Ca ratios and a decrease in Sr/(Mg + Ca) ratios, and at the same time, the variability of δ^{26}Mg values in the carbonates decreased rapidly to −2.8‰ (Fig. 8), which is interpreted as the δ^{26}Mg value of dolomite in equilibrium with modern seawater. Given that the dolostones from the Shoresh section have Mg/Ca and Sr/(Mg + Ca) ratios comparable to the completely dolomitized carbonates described in Higgins et al. (2018) (Fig. 8), the effect on Mg isotope signatures from possible precursor minerals appears to have been minimal.

Rayleigh processes during dolomite precipitation in a closed or semi-closed system would remove isotopically light Mg from the water pool, increasing the δ^{26}Mg values of the evolving seawater, as well as subsequent dolomite precipitates. Bialik et al. (2018) reported that during the Albian, southern Israel was in an epicontinental platform setting, where the water body was disconnected with the open ocean due to episodic restriction, leading to changes in the δ^{26}Mg values of seawater and syn-depositional dolostones. Although the level of connectivity between the more proximal setting described in Bialik et al. (2018) and the Shoresh section documented in this study cannot be quantified, the two sections were deposited contemporaneously in the same carbonate platform system. As such, it is likely that these restriction events also influenced the Mg isotope composition of seawater at the location of deposition of the Shoresh section. The smaller range of δ^{26}Mg values of dolostones in the Shoresh section (−2.28‰ to −1.78‰) compared with coeval dolostones from southern Israel (−2.30‰ to −1.52‰; Bialik et al., 2018) indicates that the Shoresh section was less influenced by basin restriction.

Given that δ^{26}Mg values of dolomite precipitates evolve towards higher values during progressive dolomitization during a Rayleigh process, it is reasonable to ascribe the dolomite with the lowest δ^{26}Mg value from a large sample set as being in equilibrium with contemporaneous open

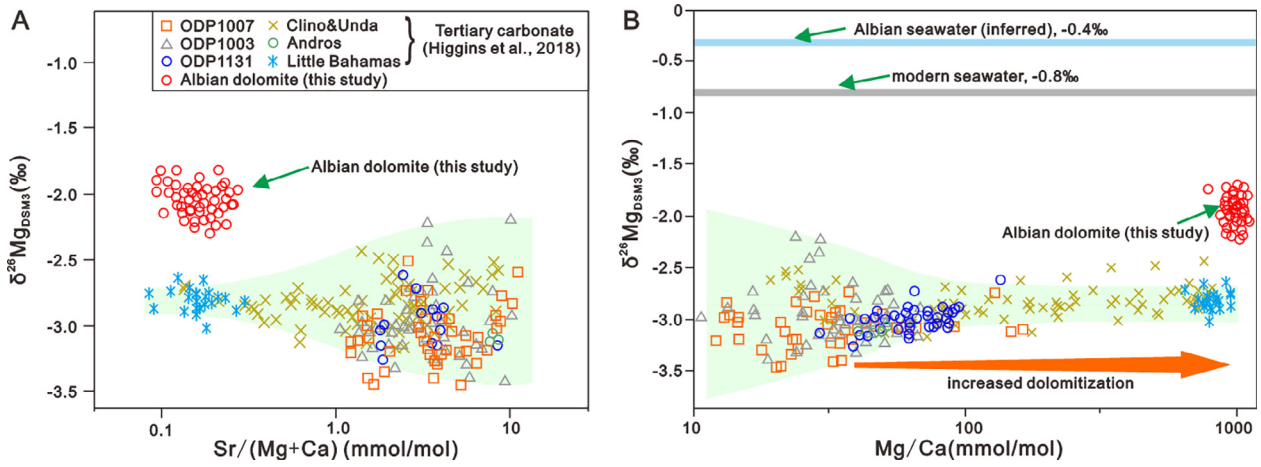

Fig. 8. Cross plots of Mg/Ca ratio versus δ^{26}Mg (A) and Sr/Ca ratio versus δ^{26}Mg (B) for variably dolomitized modern/young carbonates in Higgins et al (2018). The data for dolostones in Shoresh section is also plotted for comparison.

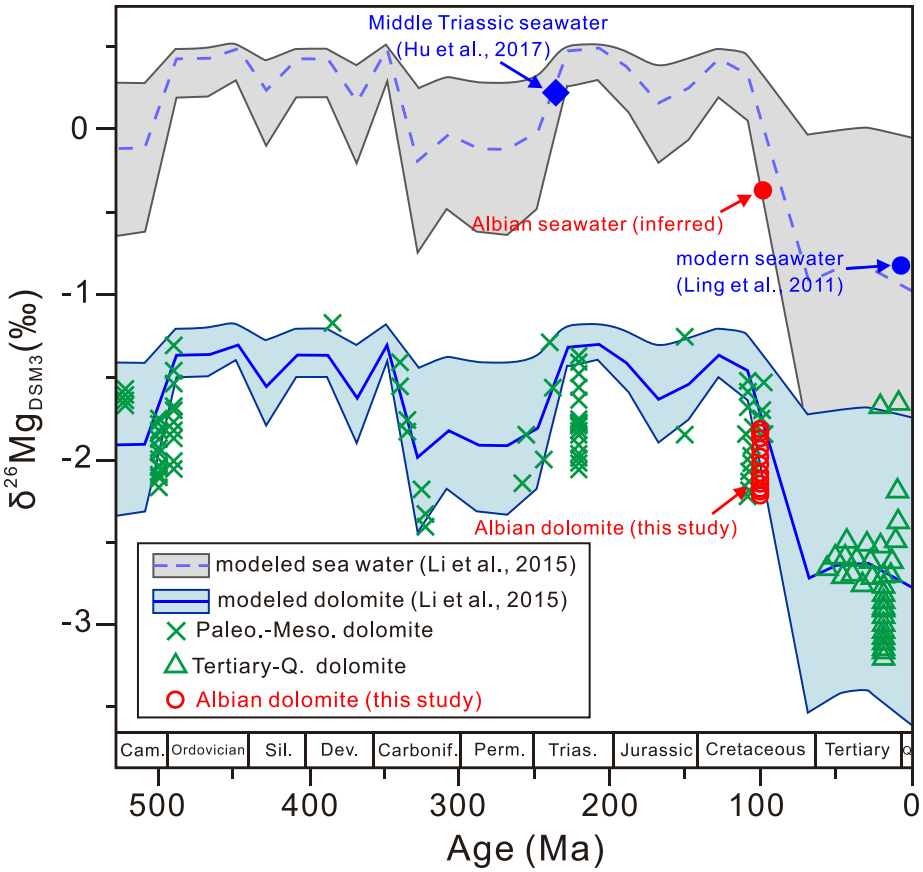

Fig. 9. Comparison of dolomite δ^{26}Mg values of Shoresh section (noted with red open circles) with the modeled Mg isotope composition curve of Phanerozoic sedimentary dolomite from Li et al. (2015). Measured dolomite Mg isotope value was selected from Galy et al. (2002), Jacobson et al. (2010), Geske et al. (2012), Azmy et al. (2013), Fantle and Higgins (2014), Geske et al. (2015a) & (2015b), Blättler et al. (2015), Lavoie et al. (2014), Hu et al. (2017), and Higgins et al. (2018). For discussions on the seawater δ^{26}Mg values, see Section 5.3.

ocean seawater. For the Albian rocks from the Shoresh section, the lowest δ^{26}Mg value is approximately −2.3‰ (Fig. 3), and this value is consistent with the study of a more proximal section of the same unit (Bialik et al., 2018). Therefore, Albian seawater would have a δ^{26}Mg value of −0.4‰, assuming a $\Delta^{26}Mg_{dolo-aq}$ fractionation factor of −1.9‰ (Li et al., 2015). The δ^{26}Mg value of Albian seawater inferred from the dolomite samples in the Shoresh section is notably higher than the δ^{26}Mg value of modern seawater (−0.8‰; Ling et al., 2011), but significantly lower than the δ^{26}Mg value of seawater in the Early Triassic (+0.3‰; Hu et al., 2017). These values confirm the prediction made by Li et al. (2015) that the Mg isotope composition of seawater has varied significantly (>1‰) during the Phanerozoic due to secular changes in global dolomitization intensity (Fig. 9). Therefore, Mg isotopes in massive sedimentary dolostones provide useful information to study past global Mg cycling and potential new insights into the climatic and tectonic history of the Earth.

6. CONCLUSIONS

In this study, we investigated well-preserved massive dolostones from the Shoresh section in the Levant margin carbonate platform of Israel to examine the effects of early diagenesis on dolomite Mg isotope signatures. The dolomites were analyzed for Mg—C—O isotopes, crystallography, and trace elements. The results revealed a negative correlation between δ^{13}C values and Mn contents, which fingerprints suboxic degradation of organic matter in the Mn(IV) reduction zone within sediments. The dolomite samples also exhibit marked variations in the degree of cation ordering and Sr contents, which are indicative of variable recrystallization after precipitation of proto-dolomite. However, δ^{26}Mg values of the dolostones are −2.01‰ ± 0.22‰ (2SD; n = 53), and do not show any correlation with δ^{13}C values, trace element contents, and dolomite lattice parameters.

In general, the behavior of Mg isotopes during diagenesis of dolomite precipitated from the Mn(IV) reduction zone is distinct from the behavior of Mg isotopes in dolomite associated with bacterial sulfate reduction and methanogenesis. This difference mainly arises from the depth of dolomitization in the sediments, which controls the accessibility of seawater Mg for the dolomitization front. In the Mn(IV) reduction zone, the sediment depth is shallow, and therefore the Mg supply from overlying seawater is not limited by diffusion, meaning that dolomite is

likely to be in equilibrium with seawater. In contrast, dolomitization in bacterial sulfate reduction or methanogenesis zones occurs at significantly greater depths, where Mg supply can be limited by diffusion, and therefore combined effects of diffusion and Rayleigh processes associated with reaction–transport would modify Mg isotopes in the dolomite. Therefore, in studies of ancient seawater chemistry based on dolomites, the depth and mechanism of dolomitization needs to be ascertained. Based on this study, dolomite formed in the Mn(VI) reduction zone has a negative correlation between $\delta^{13}C$ values and Mn contents, which is a distinctive feature that allows identification of shallow dolomitization and probable Mg isotope equilibrium between dolomite and seawater.

This study also demonstrated that recrystallization influences the elemental composition of dolomite and mineralogical parameters, but does not significantly change Mg isotopes in dolomite. This is attributed to isolation of pore water Mg from seawater during burial and the high Mg content in dolomite. This conservative behavior of Mg isotopes in dolomite requires formation of massive dolomite at shallow depths. Our study corroborates the recent work by Higgins et al. (2018), who proposed that "fluid-buffered" dolomite is in equilibrium with contemporary seawater. However, the variation in $\delta^{26}Mg$ values of the platform dolomites investigated in our study exceeds the analytical precision, implying additional process(es) to be considered in interpretation of the $\delta^{26}Mg$ values of dolostones. For this case, basin restriction is suggested as the main mechanism to introduce Mg isotope variability towards higher $\delta^{26}Mg$ values. Based on the Mg isotope record from the Shoresh section, the $\delta^{26}Mg$ value of Albian seawater is estimated to be approximately $-0.4‰$, which is intermediate between the $\delta^{26}Mg$ values for modern and Early Triassic seawater, confirming that the Mg isotope composition of seawater had changed markedly through geological history, and confirming the usefulness of Mg isotopes in tracing global Mg cycling and related geological processes.

ACKNOWLEDGEMENT

This study was jointly supported by National Science Foundation of China grant No. 41561144002 to WL and Israeli Science Foundation grant No. 44890 to NDW based on research agreements between ISF and NSFC. Additional supports to this work were provided by National Science Foundation of China grant No. 41473002 and 41622301 to WL. We thank M. Fantle, S. Riechelmann, and an anonymous reviewer for their constructive criticisms, as well as editor Fangzhen Teng for his editorial comments, this manuscript benefited remarkably from their insightful comments.

APPENDIX A. SUPPLEMENTARY DATA

Supplementary data to this article can be found online at https://doi.org/10.1016/j.gca.2019.01.029.

REFERENCES

Ahm A.-S. C., Bjerrum C. J., Blättler C. L., Swart P. K. and Higgins J. A. (2018) Quantifying early marine diagenesis in shallow-water carbonate sediments. *Geochim. Cosmochim. Acta* **236**, 140–159.

Aissaoui D. M. (1988) Magnesian calcite cements and their diagenesis dissolution and dolomitization. *Mururoa Atoll Sedimentology* **35**, 821–841.

Arkin Y., Braun M. and Starinsky A. (1965) *Type Sections of Cretaceous Formations in the Jerusalem-Bet Shemesh Area*.

Arvidson R., Guidry M. and Mackenzie F. (2011) Dolomite controls on phanerozoic seawater chemistry. *Aquat. Geochem.* **17**, 735–747.

Arvidson R. S. and Mackenzie F. T. (1999) The dolomite problem: control of precipitation kinetics by temperature and saturation state. *Am. J. Sci.* **299**, 257–288.

Azmy K., Lavoie D., Wang Z., Brand U., Al-Aasm I., Jackson S. and Girard I. (2013) Magnesium-isotope and REE compositions of Lower Ordovician carbonates from eastern Laurentia: implications for the origin of dolomites and limestones. *Chem. Geol.* **356**, 64–75.

Bar O., Gvirtzman Z., Feinstein S. and Zilberman E. (2013) Accelerated subsidence and sedimentation in the Levant Basin during the Late Tertiary and concurrent uplift of the Arabian platform: Tectonic versus counteracting sedimentary loading effects. *Tectonics* **32**, 334–350.

Barnaby R. J. and Rimstidt J. D. (1989) Redox conditions of calcite cementation interpreted from Mn and Fe contents of authigenic calcites. *Geol. Soc. Am. Bull.* **101**, 795–804.

Bertram M. A., Mackenzie F. T., Bishop F. C. and Bischoff W. D. (1991) Influence of temperature on the stability of magnesian calcite. *Am. Mineral.* **76**, 1889–1896.

Bialik O. M. and Waldmann N. (2017) The drowning of a siliciclastic shelf: insights into oceanographic reconstructions of the northern Arabian Platform during the Early Cretaceous. *Basin Res.*.

Bialik O. M., Wang X., Zhao S., Waldmann N. D., Frank R. and Li W. (2018) Mg isotope response to dolomitization in hinterland-attached carbonate platforms: outlook of δ26Mg as a tracer of basin restriction and seawater Mg/Ca ratio. *Geochimica et Cosmochimica Acta* **235**, 189–207.

Bischoff W. D., Bertram M. A., Mackenzie F. T. and Bishop F. C. (1993) Diagenetic stabilization pathways of magnesian calcites. *Carbonates Evaporites* **8**, 82–89.

Blättler C. L., Miller N. R. and Higgins J. A. (2015) Mg and Ca isotope signatures of authigenic dolomite in siliceous deep-sea sediments. *Earth Planet. Sci. Lett.* **419**, 32–42.

Broecker W. S. (1971) A kinetic model for the chemical composition of sea water. *Quat. Res.* **1**, 188–207.

Bryn Jones D. A. C. M. (1994) Comparison of geochemical indices used for the interpretation of palaeoredox conditions in ancient mudstones. *Chem. Geol.* **111**, 111–129.

Buhl D., Immenhauser A., Smeulders G., Kabiri L. and Richter D. K. (2007) Time series δ26Mg analysis in speleothem calcite: kinetic versus equilibrium fractionation, comparison with other proxies and implications for palaeoclimate research. *Chem. Geol.* **244**, 715–729.

Burdige D. J. (1993) The biogeochemistry of manganese and iron reduction in marine sediments. *Earth Sci. Rev.* **35**, 249–284.

Canfield D. E., Thamdrup B. and Hansen J. W. (1993) The anaerobic degradation of organic matter in Danish coastal sediments: Iron reduction, manganese reduction, and sulfate reduction. *Geochimica et Cosmochimica Acta* **57**, 3867–3883.

Chanda P. and Fantle M. S. (2017) Quantifying the effect of diagenetic recrystallization on the Mg isotopic composition of marine carbonates. *Geochim. Cosmochim. Acta* **204**, 219–239.

Coggon R. M., Teagle D. A. H., Smith-Duque C. E., Alt J. C. and Cooper M. J. (2010) Reconstructing past seawater Mg/Ca and Sr/Ca from mid-ocean ridge flank calcium carbonate veins. *Science* **327**, 1114–1117.

D'Hondt S., Jorgensen B. B., Miller D. J., Batzke A., Blake R., Cragg B. A., Cypionka H., Dickens G. R., Ferdelman T., Hinrichs K. U., Holm N. G., Mitterer R., Spivack A., Wang G., Bekins B., Engelen B., Ford K., Gettemy G., Rutherford S. D., Sass H., Skilbeck C. G., Aiello I. W., Guerin G., House C. H., Inagaki F., Meister P., Naehr T., Niitsuma S., Parkes R. J., Schippers A., Smith D. C., Teske A., Wiegel J., Padilla C. N. and Acosta J. L. (2004) Distributions of microbial activities in deep subseafloor sediments. *Science* **306**, 2216–2221.

Demény A., Czuppon G., Kern Z., Leél-Őssy S., Németh A., Szabó M., Tóth M., Wu C.-C., Shen C.-C., Molnár M., Németh T., Németh P. and Óvári M. (2016) Recrystallization-induced oxygen isotope changes in inclusion-hosted water of speleothems – paleoclimatological implications. *Quat. Int.* **415**, 25–32.

Demicco R. V., Lowenstein T. K., Hardie L. A. and Spencer R. J. (2005) Model of seawater composition for the Phanerozoic. *Geology* **33**, 877.

Dickson J. A. D. (2002) Fossil echinoderms as monitor of the Mg/Ca ratio of phanerozoic oceans. *Science* **298**, 1222–1224.

Elderfield H. and Schultz A. (1996) Mid-ocean ridge hydrothermal fluxes and the chemical composition of the ocean. *Annu. Rev. Earth Planet. Sci.* **24**, 191–224.

Eppelbaum L. and Katz Y. (2011) Tectonic-geophysical mapping of Israel and the eastern mediterranean: implications for hydrocarbon prospecting. *Positioning* **02**, 36–54.

Fantle M. S. and Higgins J. (2014) The effects of diagenesis and dolomitization on Ca and Mg isotopes in marine platform carbonates: implications for the geochemical cycles of Ca and Mg. *Geochim. Cosmochim. Acta* **142**, 458–481.

Farquhar G. D., Ehleringer J. R. and Hubick K. T. (1989) Carbon isotope discrimination and photosynthesis. *Ann. Rev. Plant Physiol. Plant Mol. Biol.* **40**, 503–537.

Froelich P. N., Klinkhammer G. P., Bender M. L., Luedtke N. A., Heath G. R., Cullen D., Dauphin P., Hammond D., Hartman B. and Maynard V. (1979) Early oxidation of organic matter in pelagic sediments of the eastern equatorial Atlantic: suboxic diagenesis. *Geochim. Cosmochim. Acta* **43**, 1075–1090.

Galy A., Bar-Matthews M., Halicz L. and O'Nions R. K. (2002) Mg isotopic composition of carbonate: insight from speleothem formation. *Earth Planet. Sci. Lett.* **201**, 105–115.

Gardosh M. A., Garfunkel Z., Druckman Y. and Buchbinder B. (2010) Tethyan rifting in the levant region and its role in early mesozoic crustal evolution. *Geol. Soc. Lond. Spec. Publ.* **341**, 9–36.

Geske A., Goldstein R. H., Mavromatis V., Richter D. K., Buhl D., Kluge T., John C. M. and Immenhauser A. (2015a) The magnesium isotope (δ^{26}Mg) signature of dolomites. *Geochimica et Cosmochimica Acta* **149**, 131–151.

Geske A., Lokier S., Dietzel M., Richter D. K., Buhl D. and Immenhauser A. (2015b) Magnesium isotope composition of sabkha porewater and related (Sub-) Recent stoichiometric dolomites, Abu Dhabi (UAE). *Chemical Geology* **393–394**, 112–124.

Geske A., Zorlu J., Richter D. K., Buhl D., Niedermayr A. and Immenhauser A. (2012) Impact of diagenesis and low grade metamorphosis on isotope (δ26Mg, δ13C, δ18O and 87Sr/86Sr) and elemental (Ca, Mg, Mn, Fe and Sr) signatures of Triassic sabkha dolomites. *Chem. Geol.* **332–333**, 45–64.

Goldsmith J. R. and Graf D. L. (1958) Structural and compositional variations in some natural dolomites. *J. Geol.* **66**, 678–693.

Gothmann A. M., Stolarski J., Adkins J. F., Schoene B., Dennis K. J., Schrag D. P., Mazur M. and Bender M. L. (2015) Fossil corals as an archive of secular variations in seawater chemistry since the Mesozoic. *Geochim. Cosmochim. Acta* **160**, 188–208.

Graf D. L. and Goldsmith J. R. (1956) Some hydrothermal syntheses of dolomite and protodolomite. *J. Geol.* **64**, 173–186.

Gregg J. M. and Sibley D. F. (1984) Epigenetic dolomitization and the origin of xenotopic dolomite texture. *J. Sediment. Petrol.* **54** (3), 908–931.

Grossman E. L. (2012) *Chapter 10 – Oxygen Isotope Stratigraphy, The Geologic Time Scale*. Elsevier, Boston, pp. 181–206.

Hardie L. A. (1996) Secular variation in seawater chemistry: an explanation for the coupled secular variation in the mineralogies of marine limestones and potash evaporites over the past 600 m.y. *Geology* **24**, 279–283.

Higgins J. A., Blättler C. L., Lundstrom E. A., Santiago-Ramos D. P., Akhtar A. A., Crüger Ahm A. S., Bialik O., Holmden C., Bradbury H., Murray S. T. and Swart P. K. (2018) Mineralogy, early marine diagenesis, and the chemistry of shallow-water carbonate sediments. *Geochim. Cosmochim. Acta* **220**, 512–534.

Higgins J. A. and Schrag D. P. (2010) Constraining magnesium cycling in marine sediments using magnesium isotopes. *Geochim. Cosmochim. Acta* **74**, 5039–5053.

Higgins J. A. and Schrag D. P. (2012) Records of Neogene seawater chemistry and diagenesis in deep-sea carbonate sediments and pore fluids. *Earth Planet. Sci. Lett.* **357–358**, 386–396.

Higgins J. A. and Schrag D. P. (2015) The Mg isotopic composition of Cenozoic seawater – evidence for a link between Mg-clays, seawater Mg/Ca, and climate. *Earth Planet. Sci. Lett.* **416**, 73–81.

Hips K., Haas J., Poros Z., Kele S. and Budai T. (2015) Dolomitization of Triassic microbial mat deposits (Hungary): origin of microcrystalline dolomite. *Sed. Geol.* **318**, 113–129.

Holland H. D. (2005) Sea level, sediments and the composition of seawater. *Am. J. Sci.* **305**, 220–239.

Hu Z., Hu W., Wang X., Lu Y., Wang L., Liao Z. and Li W. (2017) Resetting of Mg isotopes between calcite and dolomite during burial metamorphism: outlook of Mg isotopes as geothermometer and seawater proxy. *Geochim. Cosmochim. Acta* **208**, 24–40.

Huang K.-J., Shen B., Lang X.-G., Tang W.-B., Peng Y., Ke S., Kaufman A. J., Ma H.-R. and Li F.-B. (2015) Magnesium isotopic compositions of the Mesoproterozoic dolostones: implications for Mg isotopic systematics of marine carbonates. *Geochimica et Cosmochimica Acta* **164**, 333–351.

Huang K. J., Teng F. Z., Shen B., Xiao S., Lang X., Ma H. R., Fu Y. and Peng Y. (2016) Episode of intense chemical weathering during the termination of the 635 Ma Marinoan glaciation. *Proc. Natl. Acad. Sci. U.S.A.* **113**, 14904–14909.

Immenhauser A. and Scott R. W. (2002) An estimate of Albian sea-level amplitudes and its implication for the duration of stratigraphic hiatuses. *Sed. Geol.* **152**, 19–28.

Jacobson A. D., Zhang Z., Lundstrom C. and Huang F. (2010) Behavior of Mg isotopes during dedolomitization in the Madison Aquifer, South Dakota. *Earth and Planetary Science Letters* **297**, 446–452.

Kaczmarek S. E., Sibley D. F. and Immenhauser A. (2014) Direct physical evidence of dolomite recrystallization. *Sedimentology* **61**, 1862–1882.

Kaczmarek S. E. and Thornton B. P. (2017) The effect of temperature on stoichiometry, cation ordering, and reaction rate in high-temperature dolomitization experiments. *Chem. Geol.*.

Kasemann S. A., Pogge von Strandmann P. A. E., Prave A. R., Fallick A. E., Elliott T. and Hoffmann K.-H. (2014) Continental weathering following a Cryogenian glaciation: evidence from calcium and magnesium isotopes. *Earth Planet. Sci. Lett.* **396**, 66–77.

Katz A. and Matthews A. (1977) The dolomitization of CaCO3: an experimental study at 252–295°C. *Geochimica et Cosmochimica Acta* **41**, 297–308.

Katz M. E., Wright J. D., Miller K. G., Cramer B. S., Fennel K. and Falkowski P. G. (2005) Biological overprint of the geological carbon cycle. *Mar. Geol.* **217**, 323–338.

Land L. S. (1985) The origin of massive dolomite. *J. Geol. Educ.* **33**, 112–125.

Lavoie D., Jackson S. and Girard I. (2014) Magnesium isotopes in high-temperature saddle dolomite cements in the lower Paleozoic of Canada. *Sed. Geol.* **305**, 58–68.

Li F.-B., Teng F.-Z., Chen J.-T., Huang K.-J., Wang S.-J., Lang X.-G., Ma H.-R., Peng Y.-B. and Shen B. (2016) Constraining ribbon rock dolomitization by Mg isotopes: implications for the 'dolomite problem'. *Chem. Geol.* **445**, 208–220.

Li W., Beard B. L., Li C., Xu H. and Johnson C. M. (2015) Experimental calibration of Mg isotope fractionation between dolomite and aqueous solution and its geological implications. *Geochimica et Cosmochimica Acta* **157**, 164–181.

Li W., Chakraborty S., Beard B. L., Romanek C. S. and Johnson C. M. (2012) Magnesium isotope fractionation during precipitation of inorganic calcite under laboratory conditions. *Earth Planet. Sci. Lett.* **333–334**, 304–316.

Ling M.-X., Sedaghatpour F., Teng F.-Z., Hays P. D., Strauss J. and Sun W. (2011) Homogeneous magnesium isotopic composition of seawater: an excellent geostandard for Mg isotope analysis. *Rapid Commun. Mass Spectrom.* **25**, 2828–2836.

Liu C., Wang Z., Raub T. D., Macdonald F. A. and Evans D. A. D. (2014) Neoproterozoic cap-dolostone deposition in stratified glacial meltwater plume. *Earth Planet. Sci. Lett.* **404**, 22–32.

Machel H. G. (2004) Concepts and models of dolomitization: a critical reappraisal. *Geol. Soc. Lond. Spec. Publ.* **235**, 7–63.

Mavromatis V., Gautier Q., Bosc O. and Schott J. (2013) Kinetics of Mg partition and Mg stable isotope fractionation during its incorporation in calcite. *Geochimica et Cosmochimica Acta* **114**, 188–203.

Mavromatis V., Immenhauser A., Buhl D., Purgstaller B., Baldermann A. and Dietzel M. (2017a) Effect of organic ligands on Mg partitioning and Mg isotope fractionation during low-temperature precipitation of calcite in the absence of growth rate effects. *Geochimica Et Cosmochimica Acta* **207**, 139–153.

Mavromatis V., Meister P. and Oelkers E. H. (2014) Using stable Mg isotopes to distinguish dolomite formation mechanisms: a case study from the Peru Margin. *Chem. Geol.* **385**, 84–91.

Mavromatis V., Purgstaller B., Dietzel M., Buhl D., Immenhauser A. and Schott J. (2017b) Impact of amorphous precursor phases on magnesium isotope signatures of Mg-calcite. *Earth Planet. Sci. Lett.* **464**, 227–236.

McKenzie J. A., Hsu K. J. and Schneider J. F. (1980) Movement of subsurface waters under the Sabkha, Abu Dhabi, USE, and its relation to evaporative dolomite genesis. *SEPM Spec. Publ.* **28**, 11–30.

Morel F. M. M., Reinfelder J. R., Roberts S. B., Chamberlain C. P., Lee J. G. and Yee D. (1994) Zinc and carbon co-limitation of marine phytoplankton. *Nature* **369**, 740–742.

Paul D., Skrzypek G. and Forizs I. (2007) Normalization of measured stable isotopic compositions to isotope reference scales–a review. *Rapid Commun. Mass Spectrom.* **21**, 3006–3014.

Petrash D. A., Bialik O. M., Bontognali T. R. R., Vasconcelos C., Roberts J. A., McKenzie J. A. and Konhauser K. O. (2017) Microbially catalyzed dolomite formation: from near-surface to burial. *Earth Sci. Rev.* **171**, 558–582.

Petrash D. A., Lalonde S. V., González-Arismendi G., Gordon R. A., Méndez J. A., Gingras M. K. and Konhauser K. O. (2015) Can Mn–S redox cycling drive sedimentary dolomite formation? A hypothesis. *Chem. Geol.* **404**, 27–40.

Pinilla C., Blanchard M., Balan E., Natarajan S. K., Vuilleumier R. and Mauri F. (2015) Equilibrium magnesium isotope fractionation between aqueous Mg2+ and carbonate minerals: insights from path integral molecular dynamics. *Geochimica et Cosmochimica Acta* **163**, 126–139.

Pogge von Strandmann P. A. E., Forshaw J. and Schmidt D. N. (2014) Modern and Cenozoic records of seawater magnesium from foraminiferal Mg isotopes. *Biogeosciences* **11**, 5155–5168.

Qing H., Bosence D. W. J. and Rose E. P. F. (2001) Dolomitization by penesaline sea water in Early Jurassic peritidal platform carbonates, Gibraltar, western Mediterranean. *Sedimentology* **48**, 153–163.

Riechelmann S., Buhl D., Schröder-Ritzrau A., Spötl C., Riechelmann D. F. C., Richter D. K., Kluge T., Marx T. and Immenhauser A. (2012) Hydrogeochemistry and fractionation pathways of Mg isotopes in a continental weathering system: lessons from field experiments. *Chem. Geol.* **300–301**, 109–122.

Riechelmann S., Mavromatis V., Buhl D., Dietzel M., Eisenhauer A. and Immenhauser A. (2016) Impact of diagenetic alteration on brachiopod shell magnesium isotope (δ 26 Mg) signatures: experimental versus field data. *Chem. Geol.* **440**, 191–206.

Riechelmann S., Mavromatis V., Buhl D., Dietzel M., Hoffmann R., Jöns N., Kell-Duivestein I. and Immenhauser A. (2018) Echinoid skeletal carbonate as archive of past seawater magnesium isotope signatures – potential and limitations. *Geochimica et Cosmochimica Acta* **235**, 333–359.

Ries J. B. (2006) Mg fractionation in crustose coralline algae: Geochemical, biological, and sedimentological implications of secular variation in the Mg/Ca ratio of seawater. *Geochimica et Cosmochimica Acta* **70**, 891–900.

Rodriguez-Blanco J. D., Shaw S. and Benning L. G. (2015) A route for the direct crystallization of dolomite. *Am. Mineral.* **100**, 1172–1181.

Rosenfeld A. and Hirsch F. (2005) The Cretaceous of Israel. In *Geological Framework of the Levant – Volume II: The Levantine Basin and Israel* (eds. J. K. Hall, V. A. Krasheninnikov, F. Hirsch, C. Benjamini and A. Flexer). Historical Productions-Hall, Jerusalem, pp. 394–436.

Royse C. F., Wadell J. J. S. and Petersen L. E. (1971) X-ray determination of calcite-dolomite: an evaluation. *J. Sediment. Petrol.* **41**, 483–488.

Rustad J. R., Casey W. H., Yin Q.-Z., Bylaska E. J., Felmy A. R., Bogatko S. A., Jackson V. E. and Dixon D. A. (2010) Isotopic fractionation of Mg^{2+}(aq), Ca^{2+}(aq), and Fe^{2+}(aq) with carbonate minerals. *Geochim. Cosmochim. Acta* **74**, 6301–6323.

Sass E. and Bein A. (1982) The cretaceous carbonate platform in Israel. *Cretac. Res.* **3**, 135–144.

Sass E. and Katz A. (1982) The origin of platform dolomites: new evidence. *Am. J. Sci.* **282**, 1184–1213.

Saulnier S., Rollion-Bard C., Vigier N. and Chaussidon M. (2012) Mg isotope fractionation during calcite precipitation: an experimental study. *Geochimica et Cosmochimica Acta* **91**, 75–91.

Schauble E. A. (2011) First-principles estimates of equilibrium magnesium isotope fractionation in silicate, oxide, carbonate and hexaaquamagnesium(2+) crystals. *Geochim. Cosmochim. Acta* **75**, 844–869.

Schott J., Mavromatis V., Fujii T., Pearce C. R. and Oelkers E. H. (2016) The control of carbonate mineral Mg isotope composition by aqueous speciation: theoretical and experimental modeling. *Chem. Geol.* **445**, 120–134.

Shannon R. D. (1976) Revised effective ionic radii and systematic studies of interatomic distances in halides and chalcogenides. *Acta Cryst. A* **32**, 751–767.

Shen B., Dong L., Xiao S., Lang X., Huang K., Peng Y., Zhou C., Ke S. and Liu P. (2016) Molar tooth carbonates and benthic methane fluxes in Proterozoic oceans. *Nat. Commun.* **7**, 10317.

Sibley D. F., Dedoes R. E. and Bartlett T. R. (1987) Kinetics of dolomitization. *Geology* **15**, 1112–1114.

Teng F.-Z. (2017) Magnesium isotope geochemistry. *Rev. Mineral. Geochem.* **82**, 219.

Thamdrup B., Fossing H. and BarkerJørgensen B. (1994) Manganese, iron, and sulfur cycling in a coastal marine sediment, Aarhus Bay, Denmark. *Geochim. Cosmochim. Acta* **58**, 5115–5129.

Tipper E., Galy A., Gaillardet J., Bickle M., Elderfield H. and Carder E. (2006) The magnesium isotope budget of the modern ocean: constraints from riverine magnesium isotope ratios. *Earth Planet. Sci. Lett.* **250**, 241–253.

Vahrenkamp V. C. and Swart P. K. (1990) New distribution coefficient for the incorporation of strontium into dolomite and its implications for the formation of ancient dolomites. *Geology* **18**(5), 387–391.

Walter B. F., Immenhauser A., Geske A. and Markl G. (2015) Exploration of hydrothermal carbonate magnesium isotope signatures as tracers for continental fluid aquifers, Schwarzwald mining district. *SW Germany Chem. Geol.* **400**, 87–105.

Wang W., Qin T., Zhou C., Huang S., Wu Z. and Huang F. (2017) Concentration effect on equilibrium fractionation of Mg-Ca isotopes in carbonate minerals: Insights from first-principles calculations. *Geochimica et Cosmochimica Acta* **208**, 185–197.

Wang Z., Hu P., Gaetani G., Liu C., Saenger C., Cohen A. and Hart S. (2013) Experimental calibration of Mg isotope fractionation between aragonite and seawater. *Geochimica et Cosmochimica Acta* **102**, 113–123.

Wedepohl K. H. (1995) The composition of the continental crust. *Geochimica et Cosmochimica Acta* **59**, 1217–1232.

Wilkinson B. H. and Algen T. J. (1989) Sedimentary carbonate record of calcium-magnesium cycling. *Am. J. Sci.* **289**, 1158–1194.

Wilkinson B. H. and Algeo T. J. (1989) Sedimentary carbonate record of calcium-magnesium cycling. *Am. J. Sci.* **289**, 1158–1194.

Ziegler M. A. (2001) Late Permian to Holocene paleofacies evolution of the Arabian Plate and its hydrocarbon occurrences. *GeoArabia* **6**, 445–504.

Associate editor: Fang-Zhen Teng